Characterization of a Hydraulically Induced Bedrock Fracture

Ryan A. Brandon

Thesis submitted to the faculty of the Virginia Polytechnic Institute and State University
in partial fulfillment of the requirements for the degree of

Master of Science
In
Geosciences

Thomas J. Burbey
Kevin J. McGuire
Madeline E. Schreiber

June 13, 2014
Blacksburg, VA

Keywords: fractured bedrock aquifer, hydraulic fracturing, hydrogeologic characterization, pumping test, tracer test

Characterization of a Hydraulically Induced Bedrock Fracture

Ryan A. Brandon

ABSTRACT

Hydraulic fracturing is a controversial practice because of concerns about environmental impacts due to its widespread use in recovering unconventional petroleum and natural gas deposits. However, water-only hydraulic fracturing has been used safely and successfully for many years to increase the permeability of aquifers used for drinking and irrigation water supply. This process extends and widens existing bedrock fractures, allowing groundwater storage to increase. Researchers have studied the behavior of fractured-rock aquifers for decades, but little has been published on the hydraulic and mechanical properties of hydraulically enhanced fractures.

In this study, a multi-faceted approach consisting of aquifer and tracer testing is used to estimate the transmissivity and storage coefficient of a hydraulically induced fracture and observe its behavior as a contaminant flow pathway. The results of the aquifer tests indicated a decrease in both the transmissivity and storage coefficient of the fracture of three orders of magnitude after cessation of pumping. The aquifer temporarily experienced incomplete recovery following pumping tests, likely due to slow recharge. After complete recovery occurred, subsequent tests showed that these hydraulic properties returned to their original values, indicating elastic compression of the fracture during periods of applied stress. The results of the tracer test indicated rapid, uniform, one-dimensional flow through the fracture, with average fluid velocity approaching 1 km/day in an induced steady flow field of 6×10^{-5} m^3/s (1 gal/min) and a fracture volume of 0.238 m^3 (63 gal).

The complex heterogeneity of fractured-rock aquifers necessitates the use of multiple lines of testing in order to arrive at a detailed description of the behavior of these systems. This study demonstrates one effective method of investigating a single fracture that can uncover information about the behavior of a hydraulically enhanced aquifer that is otherwise difficult to obtain.

Table of Contents

List of Appendices

List of Figures

List of Tables

Introduction

1. Background

Hydraulic fracturing has recently emerged as a socially sensitive issue due to its controversial usage in the development of unconventional oil and gas deposits. Although not a new technology (hydraulic fracturing has been in existence in one form or another since the 1860s [AOGHS, 2014]), the recent widespread advent of horizontal drilling and slickwater fracturing, in which various chemical additives are included in the injection process in order to increase the production rate of oil or natural gas, has brought scrutiny upon the energy industry, particularly from environmentalists and state and federal governmental agencies [USDOE, 2014]. Concern has also been expressed regarding the large volumes of water consumed in hydraulic fracturing jobs and the resulting potential depletions of both surface and groundwater resources.

Despite the controversy surrounding its use in unconventional resource development, hydraulic fracturing has been used as an effective tool for enhancing the permeability of fractured bedrock aquifers and, consequently, the long-term yield of municipal and homeowner supply wells. Its attractiveness stems from the fact that it is much less expensive to "frack" an existing well than to drill a new well without the assurance of attaining a desirable yield [Banks et al., 1996]. Typically, in these applications water is the only fluid injected into the subsurface, with solid proppants (sand or ceramic particles) occasionally added to hold open a newly created fracture once the pressurized injection process ceases.

To date, no research has yet been published that hydraulically characterizes enhanced fractures, specifically, and with the increase in the use of hydraulic fracturing to provide improved well yields, especially in rural areas, it is important to understand how these enhanced

fractures behave as active groundwater flow pathways. Conversely, there is a wealth of information available related to aquifer and tracer testing in naturally fractured bedrock aquifers, but certain differences in the fracture origination process in a "fracked" aquifer lead us to hypothesize that an enhanced fracture will behave differently than a natural fracture.

These differences include the size, magnitude, and timescale of the stress field applied to the bedrock. First, natural fractures generally form as a result of a regional stress field, often related to either extensional or compressional stress from normal or reverse faulting. These stress fields are applied over relatively extended time fields. Once fracturing occurs, the stress is maintained on the aquifer, often causing migration of the solid bedrock blocks which allows the fracture to be held open by uneven wall mating [Berkowitz, 2002].

However, hydraulic fracturing procedures target specific zones within a well, and thus only apply stress to specific depths of an aquifer at any given time. The timescale of the applied stress is much shorter and, often on the order of seconds or minutes. Once the stress is removed, the fracture can quickly collapse on its walls unless the fracturing process developed a sufficient amount of asperities upon which the fracture walls can rest. If a proppant is used in the procedure, this collapse is often avoided, as the solid grains act as artificial asperities. We expect these differences in fracture origin to manifest themselves in an enhanced fracture through amplified rates of compression under hydraulic stress and an ensuing decrease in fracture transmissivity and storage.

The objective of this study was, thus, to determine the effects of inducing hydraulic stress on an enhanced fracture and how an enhanced fracture behaves as a contaminant pathway. Two types of tests were used to accomplish this objective. The first was a pumping test using packers to seal off the fracture of interest in each well. The fracture was located in each borehole using

optical televiewer and heat pulse flowmeter logs to both visually and hydraulically confirm the depths at which the packers should be placed. The pumping test results allowed transmissivity, storage coefficient, and flow dimension to be calculated. In order to ensure the validity of the results, Darcy's Law must be confirmed as valid at the targeted pumping rates, as the model for interpreting the pumping test results depends on this validation [Barker, 1988].

The second characterization method was an induced gradient tracer test, used to estimate the velocity and travel time of a solute plume carried by groundwater flow through the fracture. Using packers to isolate the fracture, a conservative saline tracer was injected into a steady flow field at the fracture in W-03, the upgradient well, and its breakthrough at EX-1, the pumped well, was monitored using electrical conductivity as a proxy for solute concentration. Information about the fracture's geometry (i.e., roughness and aperture) can be estimated using the results of this test, and effective porosity can also be measured based on combinations of possible average apertures and fracture lengths. The final result is a comprehensive look at the fracture's hydraulic and mechanical behavior by way of studying its hydraulic response to an applied stress and how it behaves as a contaminant pathway.

2. Site Description

The Fractured rock Research Site (FRS) is located in northern Floyd County, Virginia approximately 30 km southwest of Roanoke (Figure 1) (37.0463° N, -80.2024° W). The geologic setting of the site is typical of the Blue Ridge physiographic province, consisting of high relief, variable regolith thickness, and crystalline metamorphic bedrock that has been fractured and faulted at both the regional and local scales.

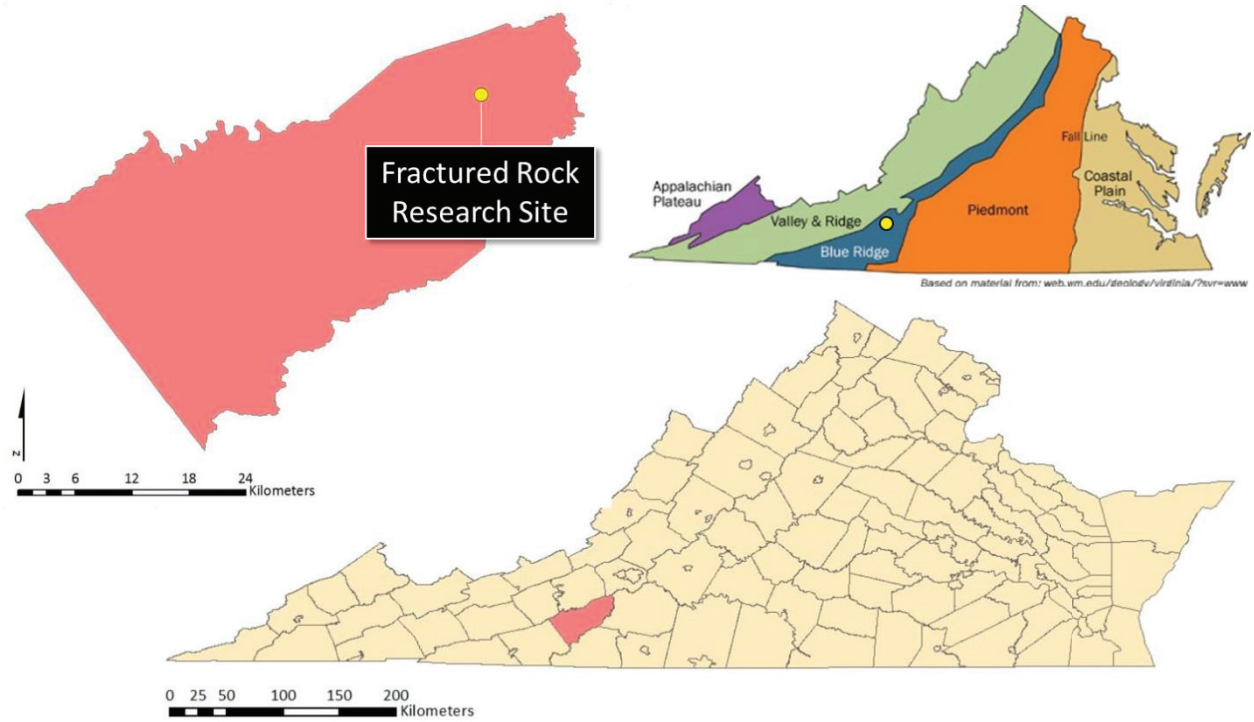

Figure 1. Site location. FRS is located in northern Floyd County, VA in the Blue Ridge physiographic province.

Bedrock predominately consists of layered Precambrian granulite, gneiss, mica schist and massive vein quartz of the Ashe Formation and is very impermeable in its competent form. The regolith varies from 0-20 m in thickness across the site and is comprised of a combination of soil and weathered bedrock (saprolite), which closely reflects the underlying parent material in composition [Buol et al., 2000]. Soil at FRS is of the Glenelg series, a well-drained, typically deep sandy clay loam and contains sand to cobble-sized fragments of unweathered bedrock which increase in frequency at greater depths [USDA, 2014].

A fractured zone is present in the bedrock due to the presence of a small thrust fault, the subcrop of which is located atop the ridge traced in red in Figure 2. At an approximate depth of

60 m this fault becomes nearly horizontal and continues past the southern end of the site (Figure 3). This fault is one in a series of *en echelon* style faults which trend southwest to northeast across the region and are associated with regional stress originating from the Blue Ridge Fault, which separates the Precambrian metamorphic rocks of the Blue Ridge from the underlying Paleozoic sedimentary formations [Seaton and Burbey, 2005].

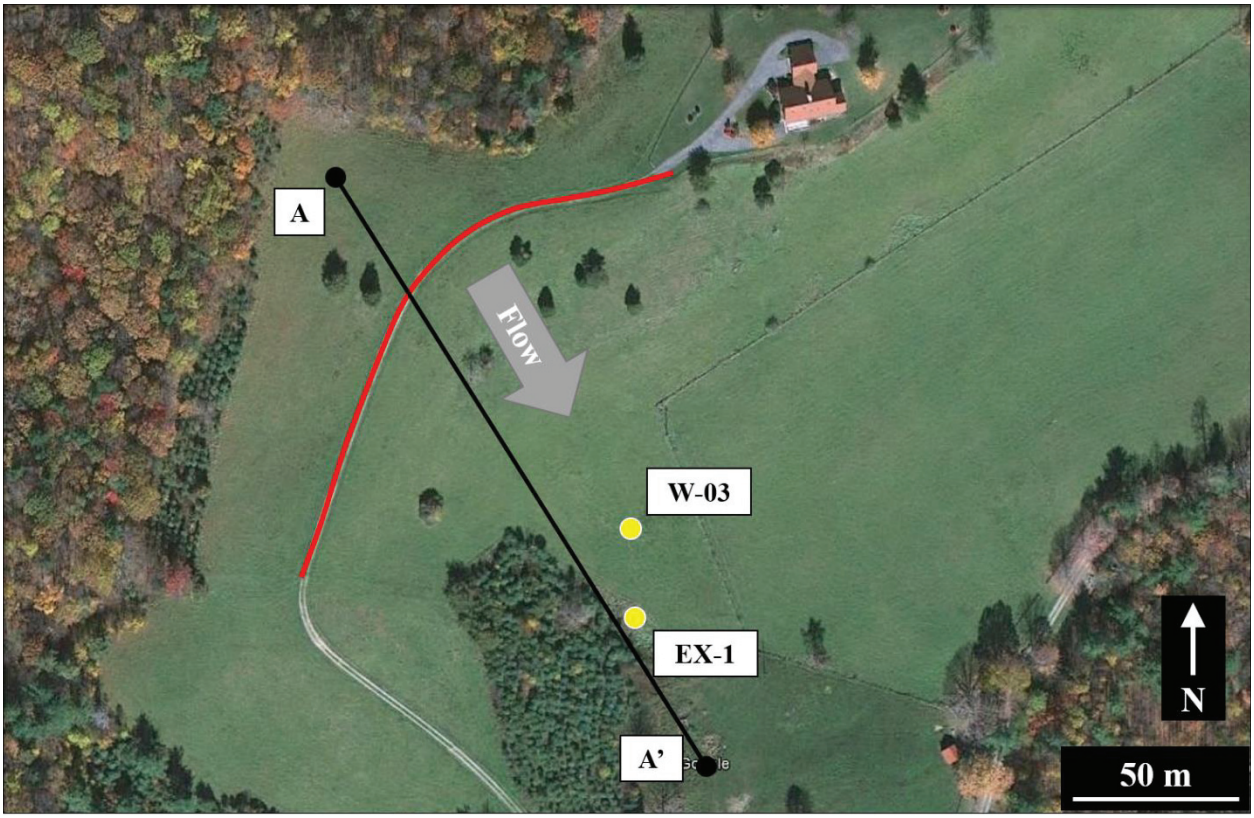

Figure 2. Aerial site image from Google Earth. Wells W-03 and EX-1 are displayed as the yellow points. The red line approximates the location of a ridge top that coincides with the subcrop of the thrust fault. A cross-section approximately following A-A' is displayed in Figure 3. The spring is located approximately at A'. The natural hydraulic gradient slopes gently to the southeast.

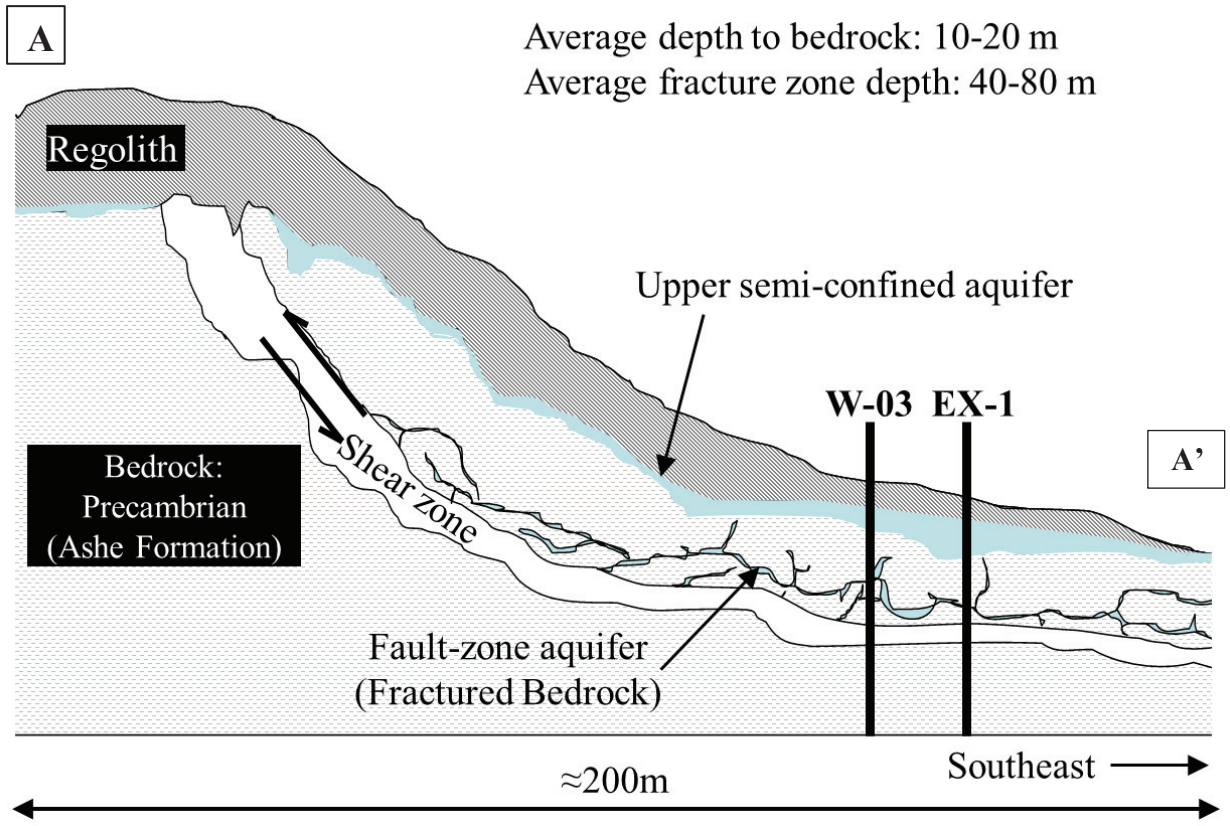

Figure 3. Cross Section A-A'. The thrust fault is the major structural feature of FRS. It is responsible for the creation of the fractured bedrock aquifer and acts as an underlying aquaclude. Most recharge to the fault-zone aquifer occurs where the shear zone meets the regolith near A. The upper semi-confined aquifer also partially recharges the lower aquifer. Modified from Burbey et al., [2011].

Two wells at the site are used in this investigation, EX-1 and W-03 (Figures 2 and 3). W-03 was one of the first wells drilled at FRS. Upon completion and development, it exhibited a strong hydraulic connection with several other wells onsite. EX-1 was drilled as part of a more recent project [Burbey et al., 2012] and demonstrated a muted, delayed hydraulic response to stresses induced in other wells upon completion. A hydraulic fracturing procedure was performed in 2008 in an attempt to increase the permeability of the well and induce a hydraulic connection with other wells at FRS.

After hydraulic fracturing of EX-1 was completed, Burbey and Zhang [2010] used both an optical televiewer probe and a heat pulse flowmeter to confirm that the wells were indeed connected. Figures 4 and 5 contain portions of these logs. The fracture studied in this investigation is located at a depth of 79.5 m below land surface in EX-1 and 62.5 m below land surface in W-03.

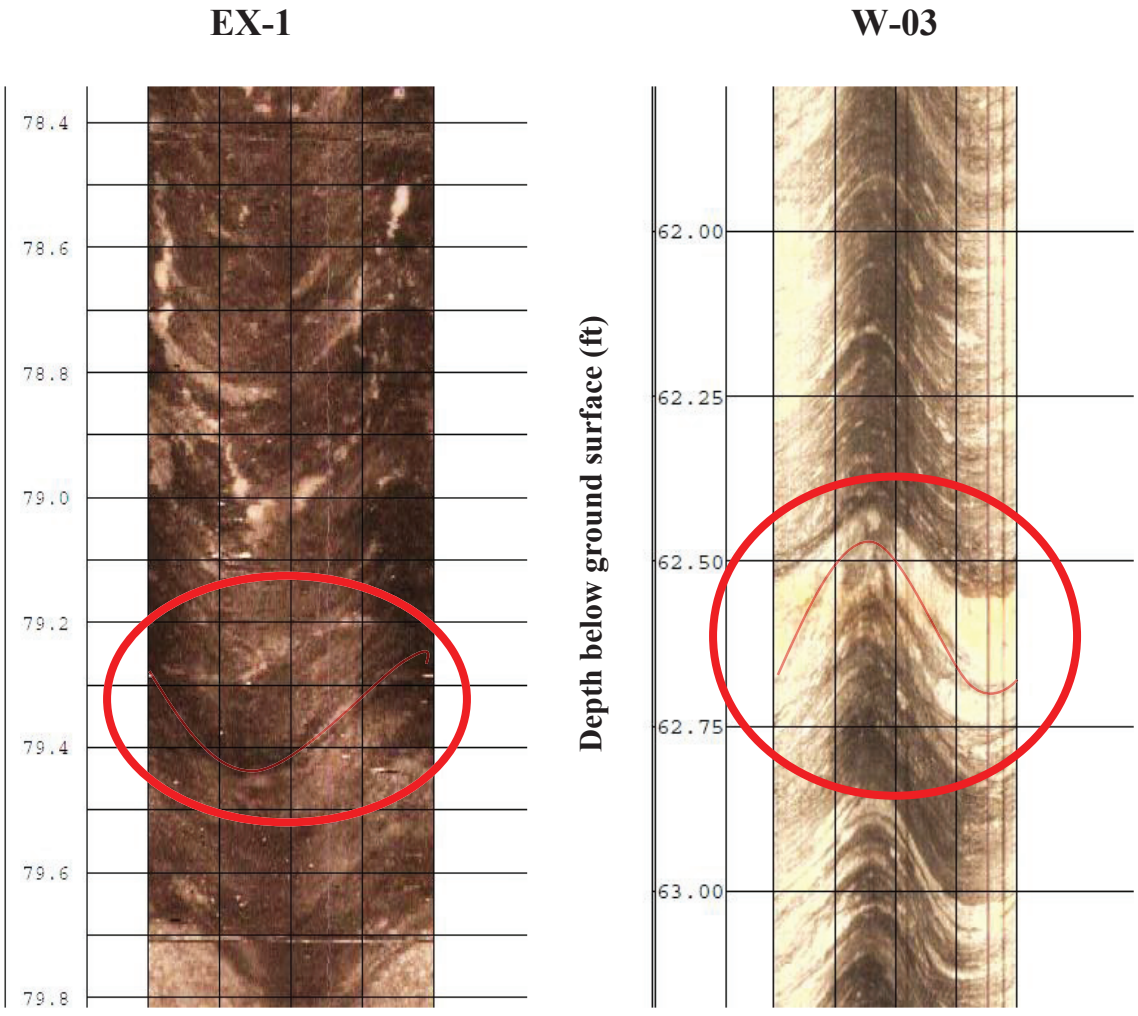

Figure 4. Optical televiewer logs of EX-1 (left) and W-03 (right). The intersections of the hydraulically active fracture with each borehole are circled in red. This imaging process displays a 360° image of the borehole wall, so the fractures are visible as faint, broken sinusoidal curves (traced in faint red) of a different amplitude and/or phase than the foliations in the host rock.

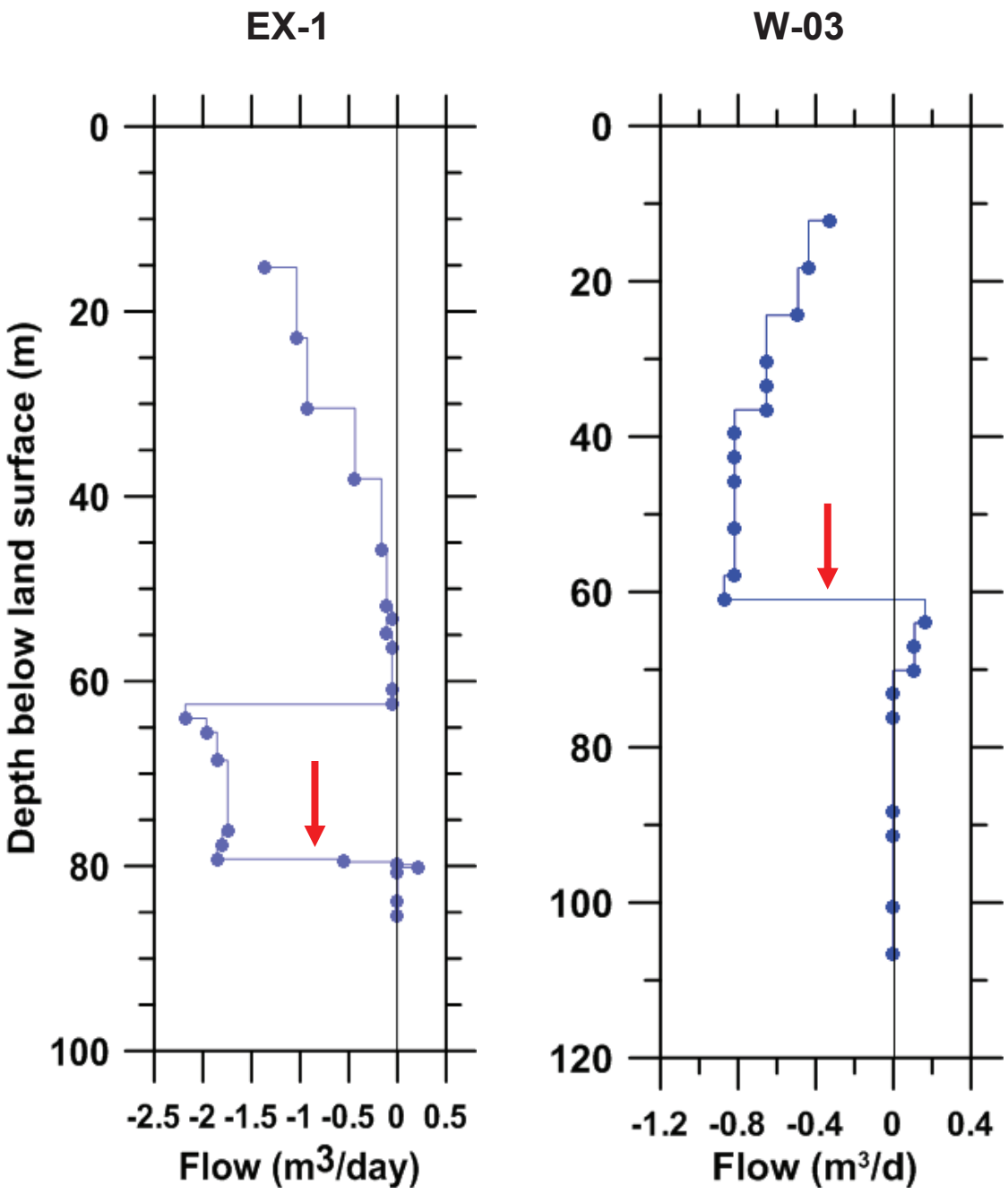

Figure 5. Heat pulse flow meter logs of EX-1 (left) and W-03 (right). These logs display a vertical profile of upward and downward flow within the borehole at discrete depths. Negative flows are downward and positive flows are upward. Data was gathered in each well individually during light pumping soon after hydraulic fracturing occurred. The fracture intersection at each borehole (red arrows) is located where downward flow suddenly ceases, as the head in the fracture was lower than the composite head of the boreholes. In EX-1 the fracture is 79.4 m bgs and in W-03 it is 62.5 m bgs. Modified from Burbey and Zhang, 2009.

The initial aquifer characterization at FRS was performed by Seaton and Burbey [2000, 2002, and 2005] using a variety of techniques including surface and borehole geophysics as well as extensive aquifer testing and CFC age dating. The previously assumed conceptual model [LeGrand, 1967] consists of a simple, homogeneous regolith layer with an extensive water table aquifer that slowly feeds the underlying fractured bedrock. Two-dimensional electrical resistivity profiles provided novel insights into Blue Ridge aquifer structure, showing that the unconsolidated zone is more heterogeneous than originally supposed. In fact, large portions of the regolith were shown to be unsaturated, contributing very little toward deep aquifer recharge [Seaton and Burbey, 2000].

An aquifer test 6 d in length was performed to evaluate transmissivity and storage values in both the bedrock and saprolite aquifers. The transmissivity of the bedrock aquifer was calculated to be on the order of 10^1 m^2/d with storage coefficients on the order of 10^{-4}. Transmissivity values in the regolith were shown to vary over three orders of magnitude (10^{-1} to 10^1) [Seaton and Burbey, 2005]. The pumping test hydrographs displayed incomplete recovery in the fractured bedrock aquifer, which suggests the testing lowered the amount of water in the system. Long-term recovery to pre-pumping levels took weeks to occur because recharge to the deep aquifer through the overlying confining unit is slow through the overlying clay and bedrock confining units. CFC age dating also revealed much faster rates of recharge to the water table aquifer compared to the deep fractured zone [Seaton and Burbey, 2005].

Gentry and Burbey [2004] studied the source of discharge at a spring located near the southern edge of FRS. Using a combination of springflow hydrograph analysis, surface geophysics, aquifer testing, and geochemical analysis, it was determined that during low flow (baseflow) conditions as much as 75% of the discharge from the spring originates in the

fractured bedrock aquifer and the remainder is discharge from the regolith aquifer. During high recharge periods, however, this ratio migrates in favor of the shallower aquifer.

White and Burbey [2007] used quantitative measurements of soil moisture, matric potential, and hydraulic conductivity to define the geologic controls on recharge processes at FRS. They combined these results with electrical resistivity data and concluded that two separate mechanisms were responsible for recharging the aquifer system at the site. Gravity-driven flow occurs where the thrust fault is nearly vertical at the ridge top and preferentially recharges the deep bedrock aquifer. High matric potentials in the soil overlying the hanging wall of the thrust fault down-gradient of the subcrop produced invalid recharge rate estimates but nevertheless illustrate another facet of the complex nature of Blue Ridge hydrogeological systems.

Preferential recharge pathways were evaluated using tracer studies in the regolith and shallow bedrock [Rugh and Burbey, 2008]. These tests confirmed the presence of preferential diffuse flow in the saprolite aquifer and fracture flow in the deep bedrock aquifer. The results also underscored the importance of geologic structure as a major contributor to heterogeneity and an important control on recharge processes in the Blue Ridge.

Aquifer mechanics has been the most recent research focus at FRS. Burbey [2010] studied the effects of Earth tides on fracture deformation and subsequent water level variations in the deep bedrock aquifer. A tiltmeter and an extensometer (both non-permanent) were installed in wells EX-1 and W-03, respectively in order to measure strains associated with aquifer testing–characteristics that are difficult to evaluate using only the results of a pumping test [Burbey et al. 2012].

Methods

Fractured rock aquifers are often extremely heterogeneous due to the nature of their origins. The only way to investigate these complex systems in detail is through multiple lines of testing. Combining hydraulic and tracer tests with an understanding of the geological processes that form these aquifers can reveal information that is otherwise intractable.

1. Validation of Darcy's Law

Before aquifer testing could commence, Darcy's Law had to be ensured to be valid in the fracture. This is because the Barker generalized radial flow model, chosen for calculating the hydraulic parameters from the drawdown data, depends on the applicability of Darcy's Law [Barker, 1988]. This not generally a concern in most hydrogeologic settings, but as fractures are open conduit-type features with a theoretical porosity of 100%, flow can be turbulent enough (Reynolds number >> 10) to render typical analysis methods invalid. In the case of turbulent flow, two possible analysis approaches are the use of an equivalent porous media model [Long et al., 1982] or treating the aquifer as a dual-flow system, where hydraulic data is analyzed as a composite of conduit and diffuse flow [Streltsova, 1988]. Both approaches require an increase in the size of the representative volume of analysis, which in the case of this study, would be counter to its objective of studying the properties of the fracture as a discrete flow pathway.

Darcy's Law states that, in viscous force-dominated flow (i.e., low Reynolds number domains), the discharge rate of water flowing through a material is proportional to the hydraulic gradient. The constant of proportionality in this relationship is referred to as the hydraulic conductivity, or K. Multiplying K by the aquifer thickness, or in the case of this study, the average aperture of the fracture, yields transmissivity, or T. This quantity is directly estimated by

applying Barker's generalized radial flow model [1988] to the drawdown time-series measured in a pumping test. Therefore, Darcy's Law must be valid for the results of the aquifer tests to be valid.

Quinn et al. [2012] performed a precise, rigorous analysis on the presence of non-Darcian flow in fractured rock using a series of rising- and falling-head pneumatic slug tests. They show that the Darcian assumption can be upheld in these aquifers for sufficiently small applied head differentials. Because of the need for the researcher to maintain constant and nearly instantaneous control over the applied pressures during these tests, pneumatic slug tests are difficult and expensive to perform. However, a good approximation of this work can be derived from Cooper and Jacob's [1946] work on graphical methods of analyzing aquifer tests in confined systems (e.g. the deep bedrock aquifer at FRS). In this method, when Darcy's Law is valid and steady flow is achieved, drawdown will plot linearly against a logarithmic time axis.

A preliminary step-drawdown test was performed at W-03 to test the validity of Darcy's Law in the fracture at a range of pumping rates. Three pumping rates were applied in succession: 1.25 gallons per minute (gpm), 2.2 gpm, and 2.9 gpm, with short recovery periods in between. The drawdown curves for each step were plotted against logarithmic time and analyzed for evidence of steady flow. The pumping periods were brief due to fast drawdown, especially at the two highest pumping rate, but steady flow did occur at all three pumping rates. When the drawdown curves are overlain, the steady flow periods align, beginning after approximately 250 s of pumping commencement (Figure 6).

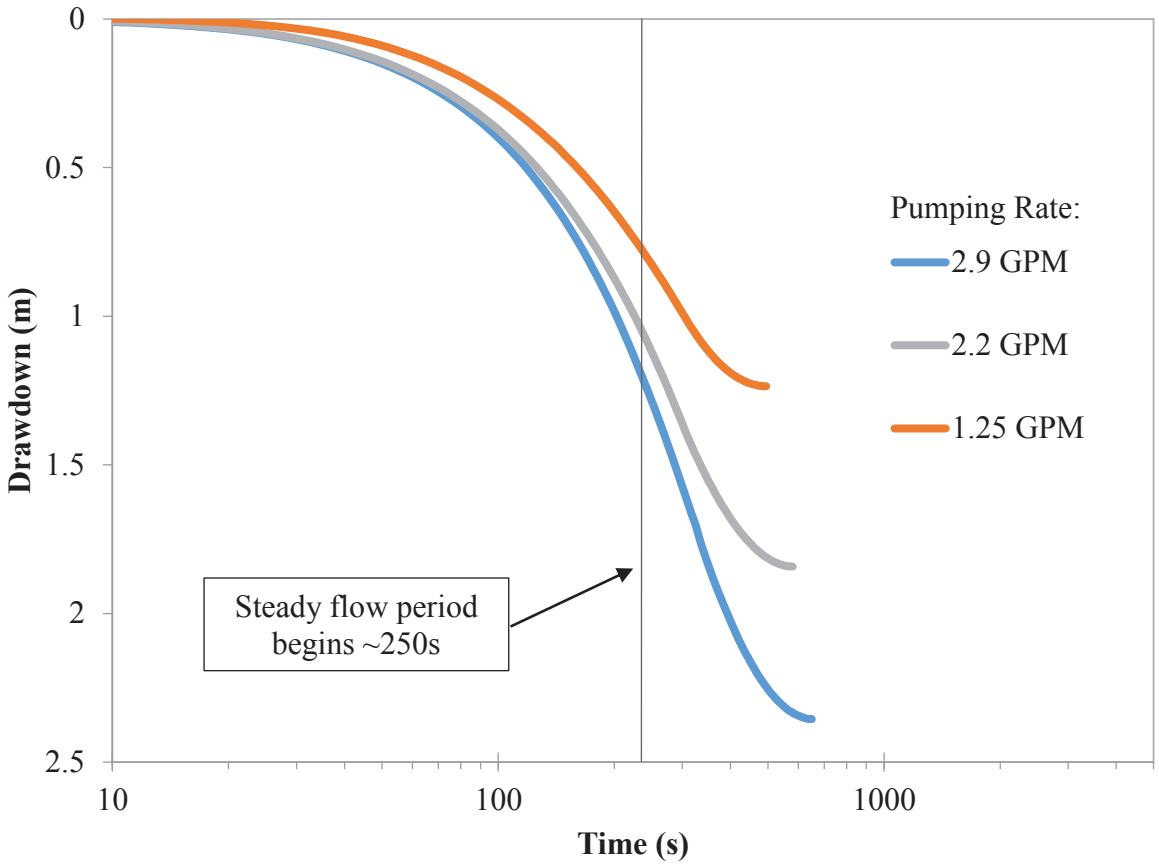

Figure 6: Darcian flow validity step test. The steps are overlain with each pumping period commencing at time zero. The straight-line portion of each step that occurs after 250 s indicates steady, Darcian-type flow within the fracture. The graphs begin to curve upward around 500 s due to cessation of pumping. This was necessary because of fast drawdown during the tests. However, steady flow can be safely assumed to continue into later times.

Darcy's Law was found to be valid at all three pumping rates. Based on the tendency of crystalline rock to produce narrow, rough fractures, this is not unexpected [Becker and Shapiro, 2003]. Friction from these rough fracture walls is likely the primary control responsible for maintaining viscous flow; as the tortuosity of the conduit increases, so does the contact area between the fluid and the fracture wall.

2. Pumping Tests

2.1 Field Procedure

Two pumping tests were performed on the isolated fracture between wells W-03 and EX-1 in order to evaluate its transmissivity and storage coefficient. The fracture was isolated using inflatable packers in each well (Figure 7), deployed in pairs to straddle the depths indicated by the heat pulse flowmeter and optical televiewer logs (62.5 m below land surface in W-03 and 79.5 m below land surface in EX-1, see Figures 4 and 5).

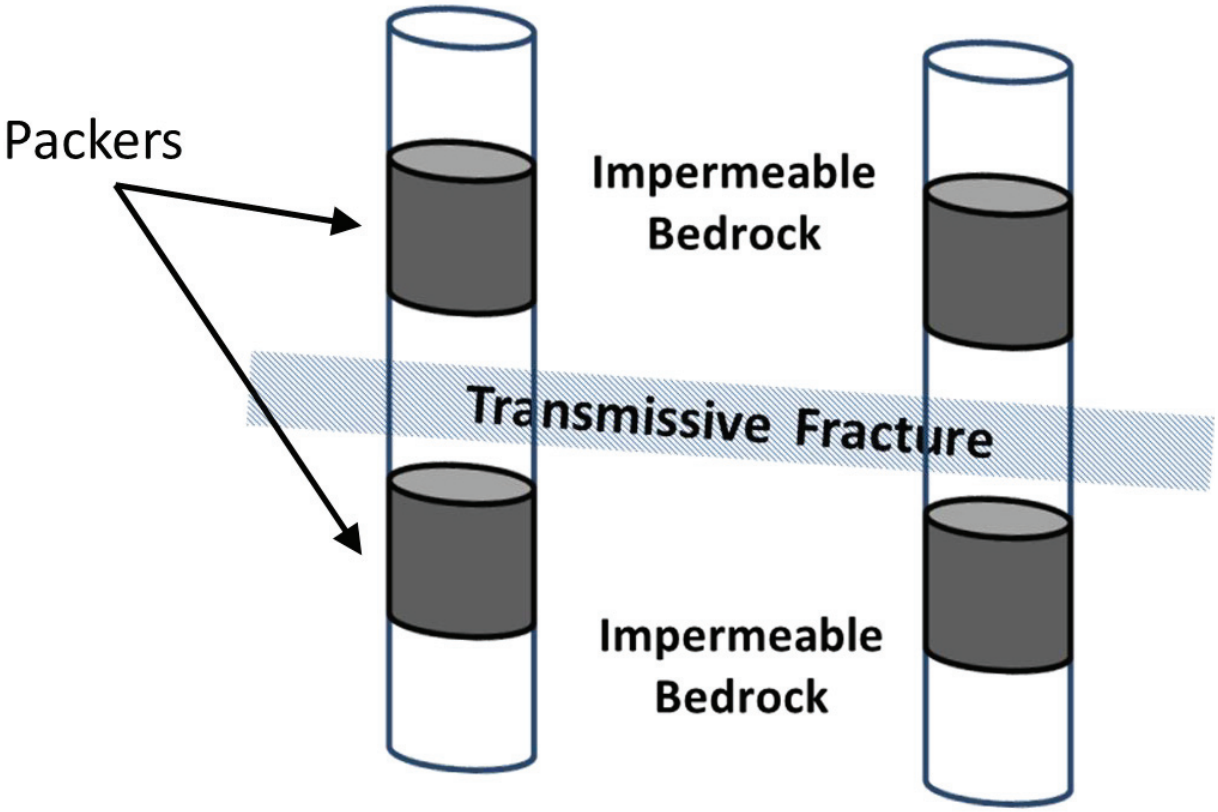

Figure 7. Packer configuration for aquifer testing. Straddle packers were used to isolate the fracture at the depths indicated in the borehole geophysical logs. A riser pipe reaching to the surface from the upper packer allowed a pressure transducer to only monitor the head from this fracture, not the typical composite head in a borehole. This configuration allows for pumping only a desired interval of the well, preventing interference from other fractures and greatly reducing borehole storage effects.

A riser pipe connected to the surface allows for pumping and monitoring to be restricted to only the isolated zone of the borehole, thereby minimizing the effects of wellbore storage on the test results. The drawdown in each well was measured for both tests using Solinst® Levelogger pressure transducers. Pumping was conducted using a 2-inch Grundfos® submersible pump with variable frequency drive.

2.2 Computational Procedure

To calculate the hydraulic parameters of the fracture, Barker's generalized radial flow (GRF) model is applied to the observed drawdown data from both tests [Barker, 1988]. This particular model was chosen for its wide range of applicability in fractured bedrock systems. The governing equation is:

$$\frac{T}{r^{n-1}}\frac{\partial}{\partial r}\left(r^{n-1}\frac{\partial h}{\partial r}\right) = S\frac{\partial h}{\partial t} \qquad (1)$$

where T is the transmissivity, r is the radial distance to the observation well, S is the storage coefficient, h is the hydraulic head, and t is time. n is the non-integral hydraulic dimension as described by Barker [1988]; when n = 1 the flow is horizontally one dimensional; when n = 2 flow is cylindrical or radial; when n = 3 flow is spherical or volumetric. The dimension can also be equal to any decimal number between these values. This allows for a greater range of fit to observed data, although it does not necessarily describe a real physical state of flow. This is generally dealt with by assuming the closest integer dimension as the true description of flow for an aquifer test.

The solution to Equation 1, reformulated for drawdown instead of head, is:

$$s(r,t) = h_0(r)\Gamma\left(\frac{n}{2} - 1, \frac{t_c(r)}{t}\right) \qquad (2)$$

where s is drawdown, which replaces h in the governing equation, and Γ is the incomplete gamma function, expressed as:

$$\Gamma(\nu, u) = \int_u^\infty e^{-t} t^{\nu-1}\, dt \qquad (3)$$

where ν and u are generic placeholder variables. For the specific Barker drawdown solution:

$$\nu = \frac{n}{2} - 1;\ u = \frac{t_c(r)}{t} \qquad (4)$$

h_0, the characteristic head, and t_c, the characteristic time, are expressed as:

$$h_0 = \frac{Q r^{2-n}}{4\pi^{\frac{n}{2}} T} \qquad (5)$$

$$t_c = \frac{S r^2}{4T} \qquad (6)$$

For each aquifer test, Q (volumetric pumping rate in m^3/s), r, s, and t are known parameters. A least squares objective function was used to optimize the parameter estimates for n, T, and S. A Mathematica® code was written to perform this analysis. The algorithm used to arrive at optimal parameter estimates is described by LeBorgne et al. [2004]. They show that the dimension parameter, n, is the most sensitive of the parameters, and should be least-squares minimized first. Then, the final optimum value of the objective function can be attained by varying transmissivity and storage.

3. Tracer Test

3.1 Field Procedure

Following the pumping tests, a forced gradient tracer test was conducted between wells W-03 and EX-1 in order to further characterize the behavior of flow within the fracture zone. A potassium bromide (KBr) tracer was selected because of its conservative nature and the lack of natural existence of Br^- in the local groundwater. Conductivity was used to measure the tracer because of its linear response to changes in bromide concentration and ease of measurement.

Background sampling was performed prior to the test on two consecutive days. Four samples were taken each day from W-03 after purging. Of the eight samples, two were reserved for calculating a conductivity-to-concentration calibration curve for Br^- (one from each sampling day), while the other six were analyzed for background bromide concentration using an Ion Chromatograph. No bromide was detected in any of the six samples.

Heads were measured in both wells using Solinst® Levelogger pressure transducers and the hydraulic gradient was directly calculated from these measurements. Fluid electrical conductivity was monitored in W-03 (the injection well) using an In-Situ® Conductivity Reel and in EX-1 (the pumped well) using a Mt. Sopris® Temperature/Conductivity probe. A conductivity-to-concentration curve was also calculated for the tracer using a Vernier® Conductivity Probe and water samples taken at the site. The conductivity measurement devices were calibrated together using a known standard solution.

The tracer test was performed with the hydraulically active fracture zones packed off in each well to eliminate interference from borehole storage and other active fractures (Figure 8). Once a steady flow rate of 6×10^{-5} m^3/s (1 gal/min) was established in the fracture, a bromide solution of 2.67 kg/m^3 (40 g KBr dissolved in 15 L water) was injected into W-03 over a period

of 2 minutes followed by a 2 minute fresh water chase injection. For the purposes of analysis, the injection is assumed to be instantaneous. The purpose of the chase injection was to completely flush the injection hose of all tracer material and ensure that the complete volume of tracer material was injected into the fracture zone in W-03. Following the injection, conductivity was monitored in W-03 to observe tracer dissipation and at the pumping well to monitor the breakthrough. The test was stopped once the conductivity levels in the pumping well had decreased to background levels again.

3.2 Computational Procedure

Maloszewski and Zuber [1990] note that a convergent radial flow tracer test in fractured rocks with negligible matrix porosity can be modeled one-dimensionally, provided the Péclet number, $Pe = vx/D_L$, has a value greater than 5, where D_L is the longitudinal dispersion coefficient, *v* is the average fluid velocity, and *x* is the flow path distance from the injection well to the monitoring well, which was calculated to be a minimum of 35.1 m based on the assumption that the fracture connection is composed of a single, straight fissure, as the actual geometry of the flow path cannot be directly evaluated. Qualitatively, this constraint on Pe requires that flow is dominated by advection rather than diffusion in order to assume one-dimensional flow within the system.

The one-dimensional form of the transport equation, which neglects transverse dispersion, and assumes that the *x*-axis is parallel to the direction of flow is:

$$D_L \frac{\partial^2 C}{\partial x^2} - v \frac{\partial C}{\partial x} = \frac{\partial C}{\partial t} \qquad (8)$$

where *C* is the tracer concentration and *t* is time. The following boundary conditions must be applied for a pumped tracer test:

$$C(x=0, t) = \frac{M}{Q}\delta(t) \quad (9)$$

$$C(x, t=0) = 0 \quad (10)$$

$$\lim_{x\to\infty} C(x, t) = 0 \quad (11)$$

where M is the mass of tracer applied, Q is the steady volumetric flow rate within the fracture, and $\delta(t)$ is the Dirac delta function, which is introduced to describe the instantaneous pulse of tracer applied to the system. Using these boundary conditions and flux-averaged concentrations, Kreft and Zuber [1978] show the non-dimensional solution of Equation 8 as:

$$C(t) = \frac{M}{Qt_0}\left[\frac{4\pi}{Pe}\left(\frac{t}{t_0}\right)^3\right]^{-\frac{1}{2}} \exp\left[-\frac{\left(1-\frac{t}{t_0}\right)^2}{\frac{4t}{Pet_0}}\right] \quad (12)$$

The non-dimensional form of the solution was chosen for this analysis because the length of the fracture is ultimately unknowable. Introducing the non-dimensional form eliminates error that would arise from the use of an incorrect length value. In this formulation, there are two unknown parameters (t_o and Pe) which can be directly estimated from the observed concentration time series. Equation 12 was fitted to the experimental data using the generalized reduced gradient algorithm in Microsoft Excel. Model goodness-of-fit was evaluated using both a minimization of the sum of squared residuals and a maximization of the model efficiency, which is:

$$E = 1 - \frac{\sum_{i=1}^{N}\left(C_f^i - C_{obs}^i\right)^2}{\sum_{i=1}^{N}\left(C_f^i - C_{avg}\right)^2} \quad (13)$$

where C_f^i and C_{obs}^i are the modeled and experimental concentrations at time t_i, and C_{avg} is the mean experimental concentration across the entire test [Nash and Sutcliffe, 1970].

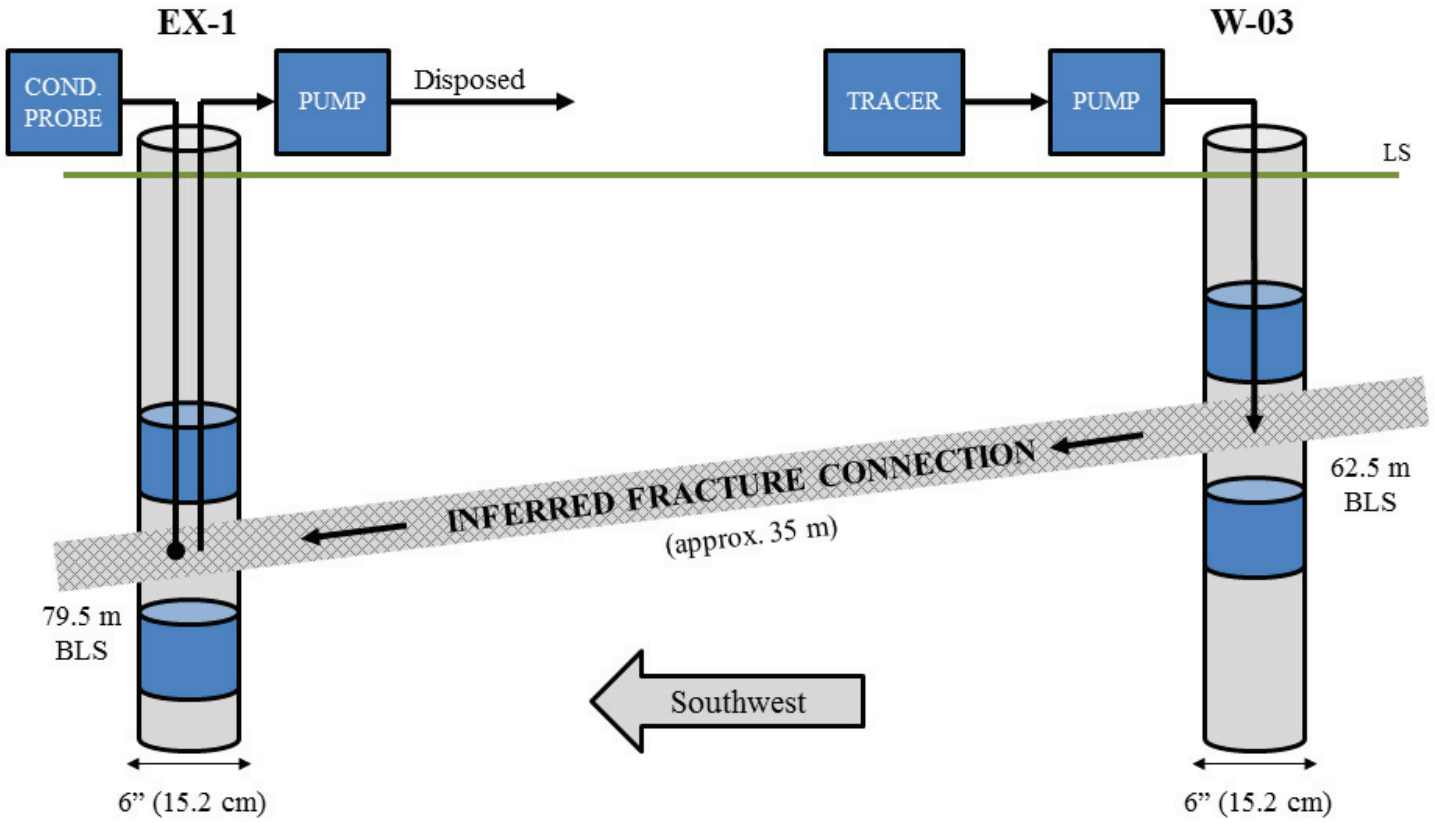

Figure 8: Diagram of induced gradient tracer test setup

Results and Discussion

1. Pumping Tests

For the first test (Figure 9), pumping was initiated in W-03 at a rate of 0.14 L/s (2.2 gpm). After six minutes, the water level in the pumping well had dropped 7 m below its initial value and the test was ended.

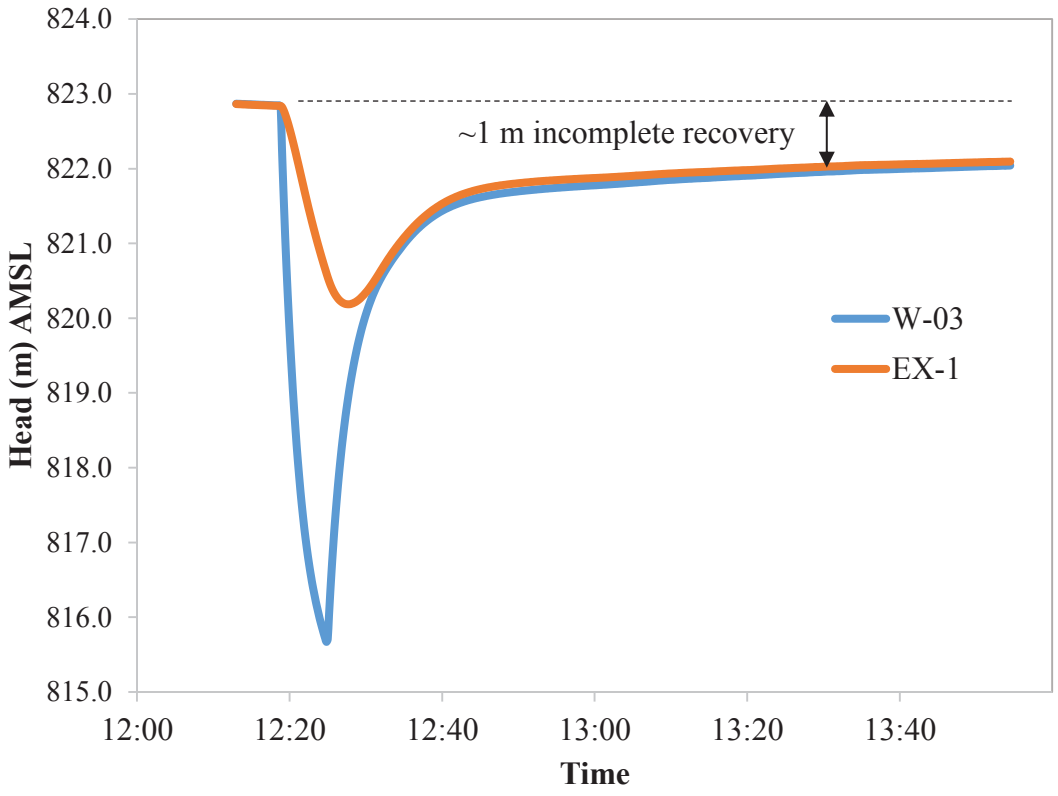

Figure 9. First pumping test. W-03 was the pumping well and EX-1 was the monitoring well. Fast drawdown caused the test to end after six minutes. Note the incomplete recovery of both wells following cessation of pumping. Time is referenced to the start of pumping.

For the second test (Figure 10), pumping was initiated in EX-1 at a rate of 0.16 L/s (2.5 gpm). After four and a half minutes, the water level in the pumping well had dropped 6 m below its initial value and the test was ended.

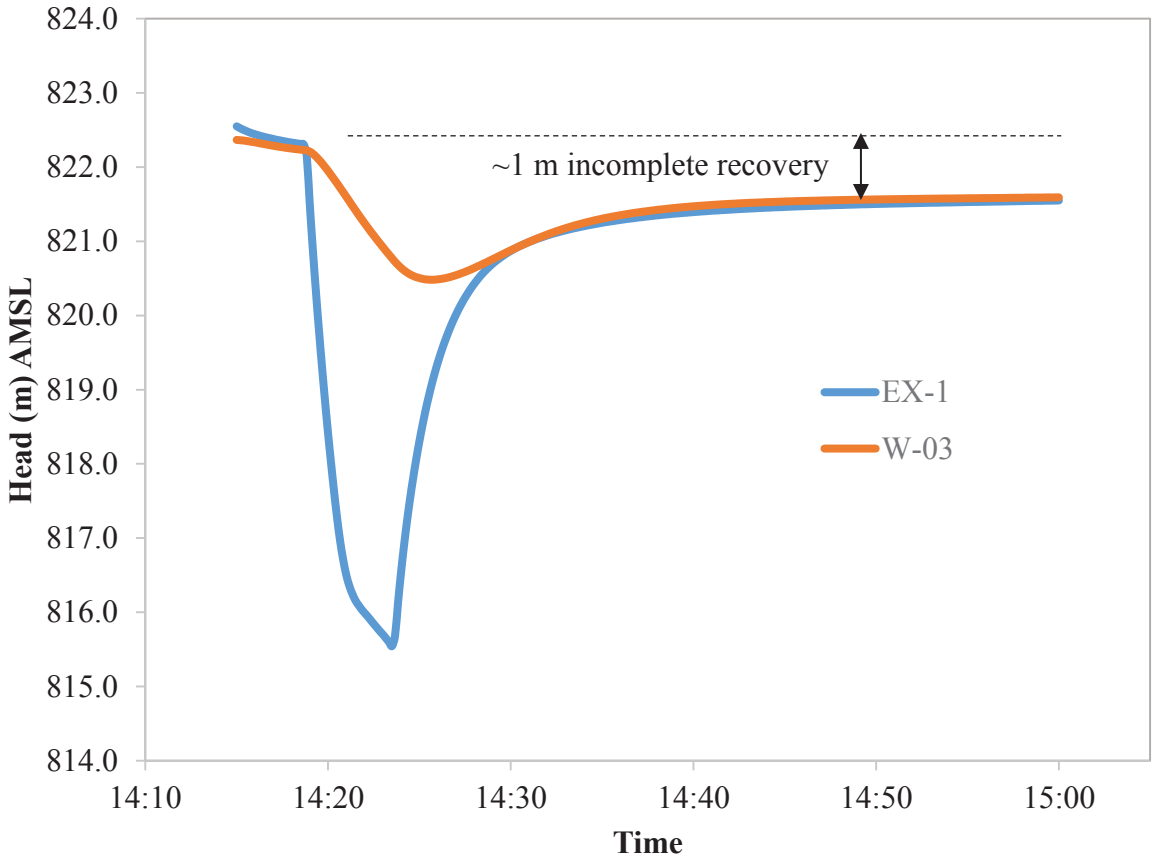

Figure 10. Second pumping test. EX-1 was the pumping well and W-03 was the monitoring well. Again, note the incomplete recovery in both wells following completion of the test.

When Barker's model is fitted to both sets of pumping test monitoring observations, a good fit is not achieved (Figure 11). The model results show a higher and earlier expected drawdown peak than what was actually observed, and recovery is poorly modeled overall. This suggests that the drawdown and recovery portions do not behave according to the same set of hydraulic parameters.

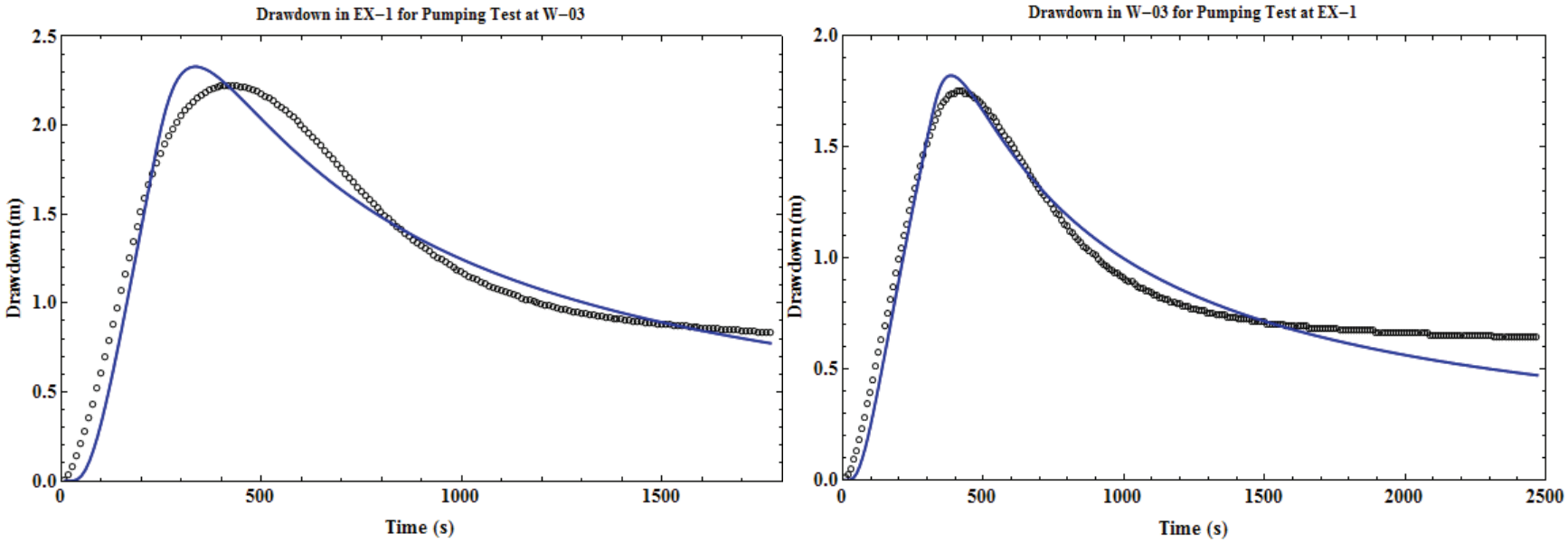

Figure 11: Barker's GRF model (blue) fitted to the observation data from each pumping test. Note the poor fit for both the drawdown peak and the overall recovery. This suggests the possibility that the drawdown and recovery portions are subject to different sets of hydraulic parameters.

In order to arrive at a more correct description of the fracture's hydraulic parameters, the drawdown and recovery portions of the observation data were separated and assessed independently. The separation point was the time at which drawdown reached its maximum value during each test. Automatic curve fitting procedures resulted in poor fits due to the tendency of a least squares optimization to treat each point as equally important to the interpretation of the results. Contrary to this point, the steady drawdown and recovery portions are more vital to understanding the nature of flow in the fracture than the early and late ends and the peaks. For this reason, manual curve fitting was used to obtain arrive at the best fit for the regions of steady drawdown and recovery.

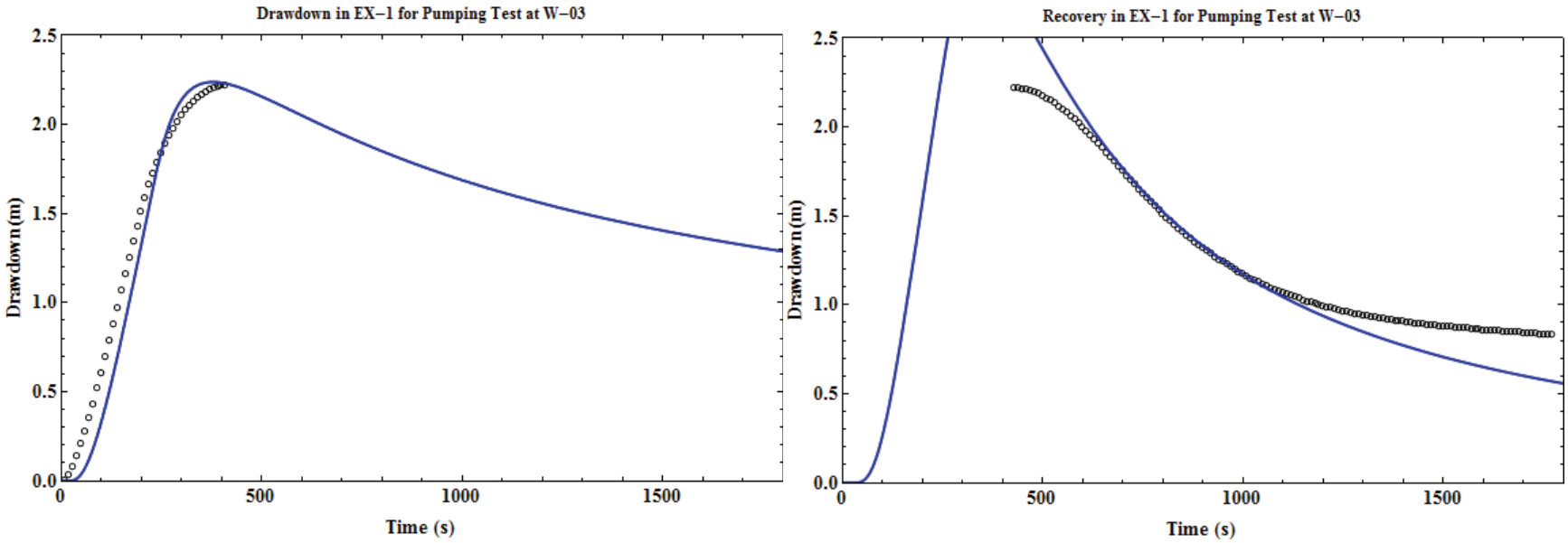

Figure 12: Drawdown and recovery in EX-1 fitted separately. The curves were fitted to match the steady drawdown and recovery periods, which provide the most accurate measure of transmissivity and storage. The model shows what recovery would look like if the fracture had access to immediate recharge. Parameter estimates and fit characteristics are shown in Table 1.

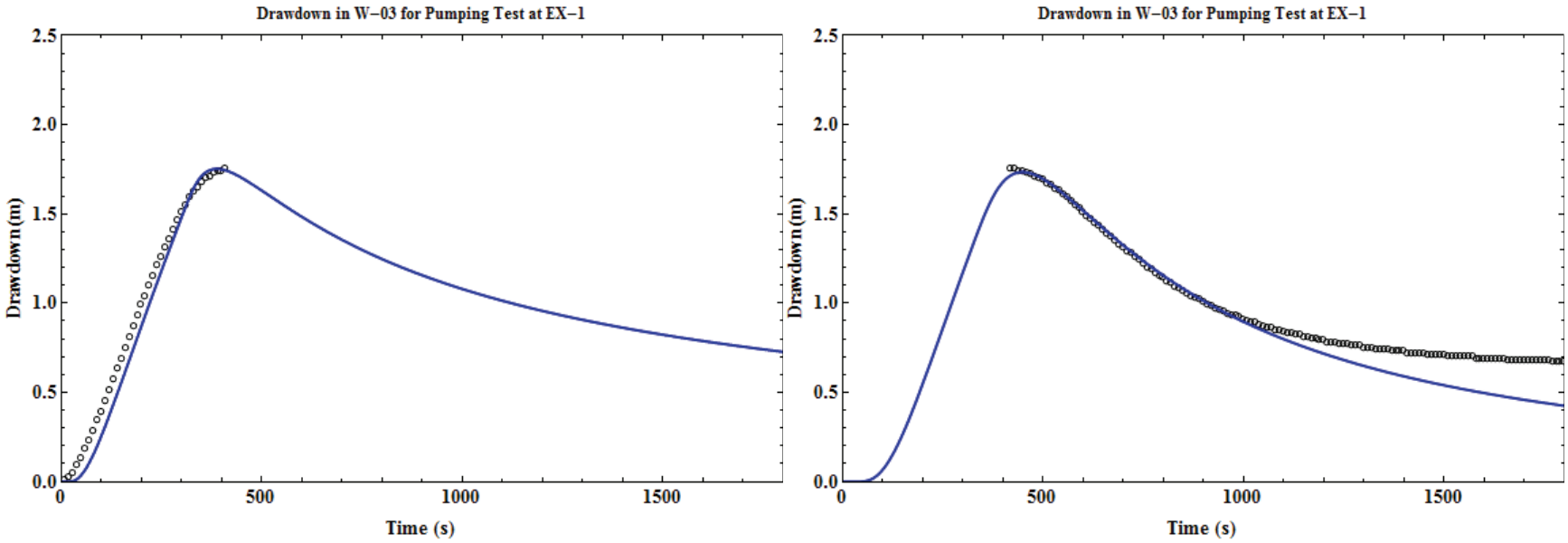

Figure 13: Drawdown and recovery in W-03 fitted separately. The curves were fitted to match the steady drawdown and recovery periods, which provide the most accurate measure of transmissivity and storage. Parameter estimates and fit characteristics are shown in Table 1.

Table 1: Summary of pumping test parameter estimates using Barker's GRF model.

Pumping Well	Observation Well	Test Period	Flow Dimension	Transmissivity (m^2/day)	Storage Coefficient
W-03	EX-1	Drawdown	1.1	8.64	6.9×10^{-5}
W-03	EX-1	Recovery	2.8	0.00449	7.9×10^{-8}
EX-1	W-03	Drawdown	1.4	3.20	2.4×10^{-5}
EX-1	W-03	Recovery	2.8	0.00432	9.2×10^{-8}

Following the initial hydraulic fracturing process in 2008, Burbey and Zhang [2010] performed pumping tests in both wells without using packers. Table 2 summarizes their results for comparison with those of this study.

Table 2. Pumping test parameters from Burbey and Zhang [2010]. These tests were performed in the wells without using packers.

Pumping Well	Observation Well	Flow Dimension	Transmissivity (m^2/day)	Storage Coefficient
W-03	EX-1	2.01	0.073	1.3×10^{-5}
EX-1	W-03	2.59	0.008	1.2×10^{-6}

An immediate observation that can be made by looking at the pumping test hydrographs in Figures 9-10 is that both wells asymptotically recover to a head lower than the initial level. It appears that the pumping tests removed water from the system, and therefore the head in the fracture does not reach its original pre-pumping level until the bedrock aquifer is recharged from the overlying saprolite aquifer. Seaton and Burbey [2005] note that this process is dependent on precipitation amounts and can occur in as quickly as a few days or as long as several weeks.

After separating the drawdown phases of each test from their respective recovery periods and analyzing them individually, flow dimension is shown to increase from approximately 1-

dimensional linear flow to nearly 3-dimensonal volumetric flow after the pump is shut off. Transmissivity and the storage coefficient decrease by 3 orders of magnitude once drawdown ceases. This is likely caused by the compression of the fracture due to the decrease in head during pumping. Burbey et al. [2012] calculated a compression rate of 0.26 μm compression for every meter of head loss using an extensometer and tiltmeter in a previous study of these wells. They also show that this compression is elastic in nature and does not permanently alter the fracture's aperture. Increased contact between asperities on the fracture wall during these compression events is likely restricting the space available to serve as a flow pathway, and thus lowers the transmissivity of the aquifer temporarily until elastic rebound occurs. Similar transmissivity and storage coefficient estimates during the drawdown phases of both pumping tests serve as further evidence of this elasticity.

This three order of magnitude change in hydraulic behavior is significant, but Berkowitz [2002] noted that some fractures have been shown to undergo a decrease in these parameters of over five orders of magnitude under sub-millimeter lengths of aperture compression.

In Burbey and Zhang's [2009] pumping tests in W-03 and EX-1, they observed that when EX-1 is being pumped, the flow dimension during drawdown is greater than when W-03 is being pumped. In their study, Burbey and Zhang concluded that this was likely caused by the fact that the fracture dips more steeply at its intersection with the borehole wall at EX-1, thereby increasing its surface area. The pumping tests for this investigation revealed the same occurrence, and since the fracture was sealed off from all other possible flow sources with packers during this pumping test, this appears to confirm their conclusions.

2. Tracer Test

The conductivity values observed in EX-1 during the test were converted to concentrations in kg/m^3 using an empirically derived calibration curve. Two background samples from W-03 were mixed with increasing amounts of KBr and their conductivity recorded. The samples were combined and fit using linear regression to determine the relationship between conductivity and bromide concentration. Equation 6 represents the linear relationship resulting from combining these data and forcing the x-intercept to a conductivity of 109 μS/cm, which was found to be the background conductivity in the monitoring well on the day of the tracer test. The regression yields an R^2 value of 0.9993.

$$Br^- \text{ Concentration}(kg/m^3) = 7.235\times10^{-4} * \text{Conductivity}(\mu S/cm) - 0.07887 \qquad (14)$$

The resulting tracer concentration time series data were plotted with time zero set as the point of tracer and chase injection completion. Figure 14 displays the plotted experimental and modeled values, and Table 4 lists the calculated model parameter values.

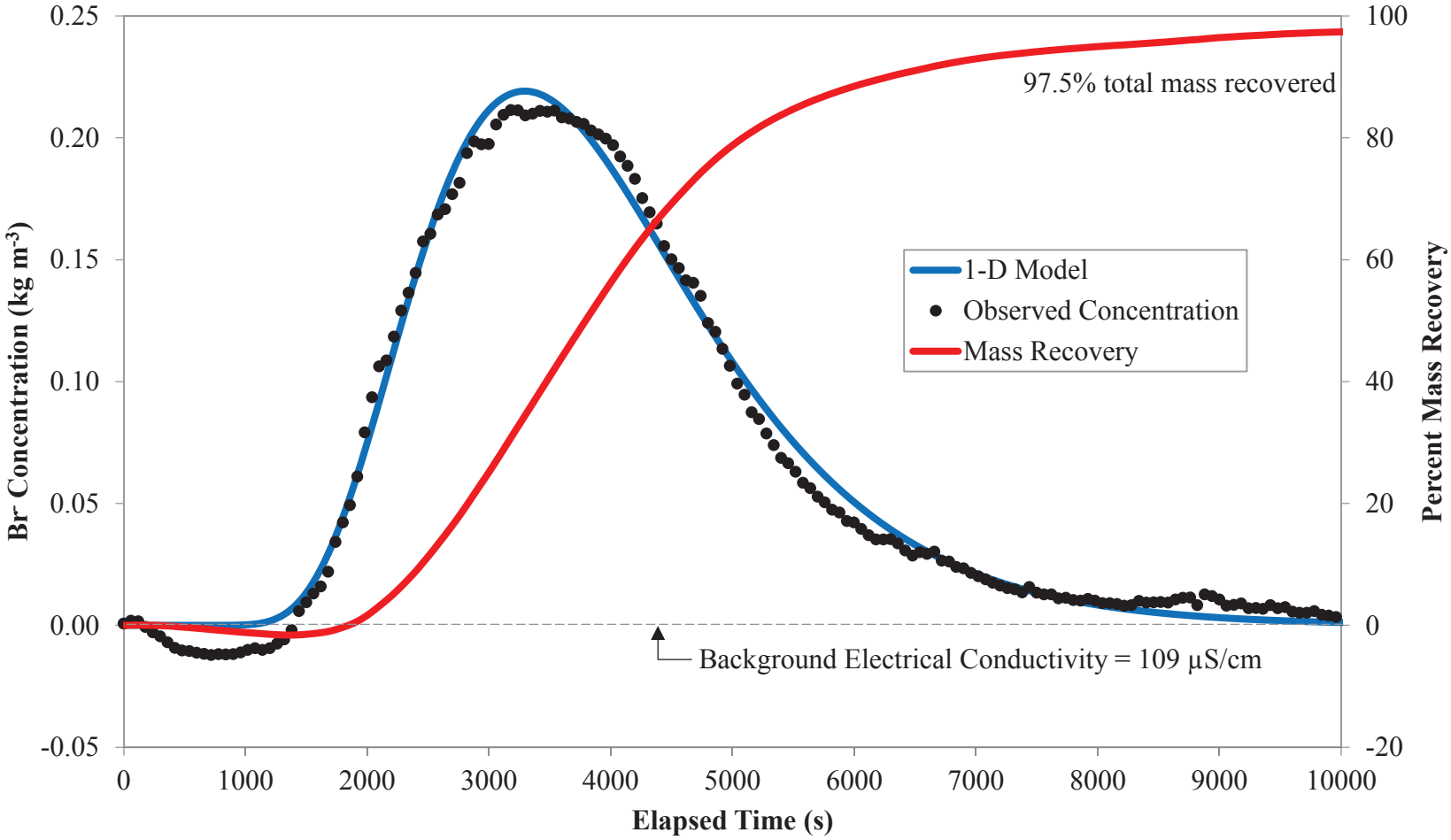

Figure 14: Experimental data with mass recovery and fitted model (Equation 12). The background conductivity was measured immediately prior to tracer injection and set as 0.00 kg/m^3 Br^- in the calibration model. The dip occurring between 100-1400 s elapsed time is likely due to the presence of recently recharged water in the fracture or borehole water of a different geochemical signature. Mass recovery is calculated from the observed concentrations and asymptotically approaches 97.5%.

Table 3: Advection-dispersion model parameter values.

Known & Assumed Parameters		
Parameter	**Value**	**Units**
M (known)	0.40	kg
Q (known)	6×10^{-5}	m^3/s
Estimated Parameters		
Pe	16.1	dimensionless
t_0	3960	s
Goodness-of-fit		
Sum of squared residuals		7.90×10^{-3}
Nash-Sutcliffe efficiency		0.992

Leibundgut et al. [2009] show that the total volume of mobile water in the system (i.e., the fracture plus the volume between each pair of packers) can be estimated as,

$$V_m = Qt_0 = 0.238\ m^3 = 62.8\ gal \qquad (15)$$

Because the volume between the packers is known (7.5 gal in each pair, for a total of 15 gal), the fracture volume can be estimated as 47.8 gal. This total volume of mobile water in the fracture was completely pumped within the first hour of the test. During the length of the test nearly three total mobile volumes were removed.

Two other parameters, D_L and v are sensitive to changes in x, the length of the fracture between the two wells. The fracture must be a minimum of 35 m long due to its apparent dip at each borehole and the known distance between the wells. These parameters are also estimated for fracture lengths of 40 and 45 m, which could be

possible in the cases of a tortuous fracture or a true dip angle that varies significantly from the apparent dip angle measured from the heat pulse flow meter logs.

Effective porosity, n_e, can also be estimated from the breakthrough data as,

$$n_e = \frac{Qt_0}{\pi x^2 H} \quad (16)$$

where x is the fracture length and H is the fracture's average aperture across the length. As both of these quantities are unknowable, Table 5 displays a range of estimates for various assumed values of x and H.

Table 4: Sensitivity of average velocity and longitudinal dispersion coefficient to changes in fracture length.

Fracture Length (m)	Average velocity (km/d)	Longitudinal Dispersion Coefficient (m^2/s)
35	0.76	0.019
40	0.87	0.025
45	0.98	0.032

Table 5: Sensitivity of effective porosity estimates to variations in fracture length and average aperture.

Average Aperture (mm)	35 m Fracture Length	40 m Fracture Length	45 m Fracture Length
0.25	0.25	0.19	0.15
0.50	0.12	0.095	0.075
1.00	0.062	0.047	0.037
2.00	0.031	0.024	0.019

For the purposes of evaluating the validity of this analysis, the calculated Pe falls above the threshold of 5 set by Maloszewski and Zuber [1990] for applying a one-dimensional form of the transport equation to describe a combined pumping-tracer test (Péclet numbers lower than 5 are indicative of diffusion-driven transport). Estimates of effective porosity for larger apertures compare favorably with the value calculated by Burbey [2009] at W-03 in a previous study (n_e = 0.02).

Several important characteristics of flow within this fracture can be described using the optimized model parameters and other derived characteristics. The mean transit time suggests that even under the slightest of induced hydraulic gradients, transport could occur on the order of hundreds of meters per day in this aquifer. This greatly increases the likelihood of long range effects caused by a pollution incident. Longitudinal dispersivity is a scale-dependent quantity, so its usefulness is restricted to the particular flow path used in the test in which it was calculated. Dividing the flow path distance by the longitudinal dispersivity yields the aforementioned Péclet number. The Péclet number suggests that, as previously assumed, flow is dominated by advective processes in this aquifer. Therefore, channelization likely occurs through only a small percentage of the aquifer, and secondary fractures would, therefore, only serve as groundwater storage features, not active pathways for flow and transport.

The steep, compressed tail of the breakthrough curve suggests rapid, uniform flow through the fracture, even at low flow rates. This implies that flow is mostly confined to discrete channels within the aquifer, as there is little indication of eddying or transient storage occurring in the flow path. Becker and Shapiro [2003] note that channeling often

occurs in deep crystalline rock environments because of the host rock's tendency to develop narrow, rough fractures.

The experimental data show that a slight decrease in measured concentration (conductivity) occurred immediately before the initial tracer breakthrough, ultimately falling below the previously measured background levels. It is possible that this occurred as a result of rapid recharge to the deep aquifer due to a period of stress (property owner usage) and subsequent precipitation in the weeks prior to the tracer test. Recently recharged water will have a lower conductivity signature than groundwater that has been in contact with the host rock for an extended period of time.

Two regions of the breakthrough curve show slight discrepancies between the observed tracer concentrations and the model. The model somewhat overestimates the maximum bromide concentration both at the peak and between 5000-6000 s elapsed time. This indicates that the fracture is not perfectly smooth and therefore flow is not completely channelized; small pockets of transient storage are likely occurring within the rougher regions of the fracture.

A relatively simple one-dimensional curve-fitting model was used to analyze the breakthrough curve for this tracer test. More complex models exist for describing mass flow within fractures, such as the transient solute storage model proposed by Raven et al. [1988]. These models might have provided a better fit to the observed bromide concentrations, but at the cost of increased uncertainty due to parameter non-uniqueness. The initial indications from the observed data that this fracture is indeed relatively smooth-walled with channelized flow afforded the opportunity to use a simpler model and therefore prevent the introduction of any unnecessary additional uncertainty.

Conclusions

Hydraulic fracturing is most commonly associated with unconventional development of oil and gas resources, but it has been used effectively to increase well yields in homeowner and municipal wells for many years. One such well, EX-1 at the Fractured Rock research Site in the Blue Ridge province, was chosen as the study point for this investigation, along with another well, W-03, with which it is now hydraulically connected as a result of a hydraulic fracturing procedure. This investigation used a multi-faceted approach of combining aquifer tests and a tracer test to characterize this fracture.

Pumping tests were conducted using inflatable packers to seal off the fracture from interference with other fractures and borehole storage. Results show that both wells undergo incomplete recovery after a pumping stress is applied. This is due to dewatering of the fracture due to the applied stress and subsequent head loss followed by a slow recharge period. In addition, transmissivity and storage decrease by three orders of magnitude after drawdown ceases, likely caused by compression of the fracture under stress. This variation compares favorably with previously studied, naturally-formed fractures.

A saline tracer test across the fracture indicates rapid, uniform flow under even the slightest of induced hydraulic gradients. There is very little evidence of transient storage and eddying in the fracture. Velocity estimates from the tracer test indicate the potential for contaminant transport at rates approaching 1 km/day.

Fractured rock aquifers are often extremely heterogeneous due to the nature of their origins. Complex patterns of deformation, such as those observed in the Blue Ridge physiographic province, often create extensive fracture networks with varying degrees of

interconnectivity to each other and overlying surficial aquifers. Hydraulic fracturing without the use of proppants appears to further augment the intricacy of these systems by introducing temporal heterogeneity in the form of amplified elastic compression rates, which alter the properties of flow within these fractures during periods of stress and recovery. An effective way of investigating these complex systems in detail is through multiple lines of testing. Combining hydraulic and tracer tests with an understanding of the geological processes that form these aquifers can reveal information that is otherwise difficult to obtain.

References

American Oil and Gas Historical Society (AOGHS) (2014), *Shooters – A Fracking History,* http://aoghs.org/oilfield-technologies/shooters-well-fracking-history, edited by B.A. Wells, accessed May 29, 2014.

Banks, D., N.E. Odling, H. Skarphagen, and E. Rohr-Torp (1996), Permeability and stress in crystalline rocks, *Terra Nova, 8,* 223-235.

Barker, J.A. (1988), A generalized radial flow model for hydraulic tests in fractured rock, *Water Resour. Res., 24*(10), 1796-1804.

Becker, M.W. and A.M. Shapiro (2003), Interpreting tracer breakthrough tailing from different forced-gradient tracer experiment configurations in fractured bedrock, *Water Resour. Res.*, *39*(1), 1024-1036.

Berkowitz, B. (2002), Characterizing flow and transport in fractured geologic media: A review, *Adv. Water Resour., 25,* 861-884.

Buol, S.W., A. Amoozegar, and M.J. Vepraskas (2000), Physical, chemical, and morphological properties of some regoliths in North Carolina, *Southeast Geology, 39*, 151-160.

Burbey, T.J. (2010), Fracture characterization using Earth tide analysis, *J. Hydrol., 380*, 237-246.

Burbey, T.J. and M. Zhang (2009), Assessing hydrofracing success from Earth tide and barometric response, *Ground Water, 48,* 825-835.

Burbey, T.J., D. Hisz, L.C. Murdoch, and M. Zhang (2012), Quantifying fractured crystalline-rock properties using well tests, earth tides and barometric effects, *J. Hydrol., 414-415,* 317-328.

Cooper, H.H., Jr. and C.E. Jacob (1946), A generalized graphical method for evaluating formation constants and summarizing well-field history, *Transactions, American Geophysical Union, 27,* 526-534.

Gentry, W.M. and T.J. Burbey (2004), Characterization of ground water flow from spring discharge in a crystalline rock environment, *J. Am. Water Resour. As., 40*(5), 1205-1217.

Kreft, A. and A. Zuber (1978), On the physical meaning of the dispersion equation and its solutions for different initial and boundary conditions, *Chem. Eng. Sci., 33*, 1471-1480.

Le Borgne, T., O. Bour, J.-R. de Dreuzy, P. Davy, and F. Tourchard (2004), Equivalent mean flow models for fractured aquifers: insights from a pumping tests scaling interpretation, *Water Resour. Res., 40,* doi: 10.1029/2003WR002436.

LeGrand, H.E. (1967), Ground water of the Piedmont and Blue Ridge provinces in the Southeastern States, *U.S. Geological Survey Circular 538*, 11 p.

Leibundgut, C., P. Maloszewski, and C. Külls (2009), *Tracers in Hydrology*, Wiley-Blackwell, 415 pp.

Long, J.C.S, J.S. Remer, C.R. Wilson, and P.A. Witherspoon (1982), Porous media equivalents for networks of discontinuous fractures, *Water Resour. Res.*, *18*(3), 645-658.

Maloszewski, P. and A. Zuber (1990), Mathematical modeling of tracer behavior in short-term experiments in fissured rocks, *Water Resour. Res.*, *26*(7), 1517-1528.

Nash, J.E. and J.V. Sutcliffe (1970), River flow forecasting through conceptual models part I – a discussion of principles, *J. Hydrol., 10*(3), 282-290.

Quinn, P., J.A. Cherry, and B.L. Parker (2012), Hydraulic testing using a versatile straddle packer system for improved transmissivity estimation in fractured-rock boreholes, *Hydrogeol. J., 20,* 1529-1547.

Raven, K.G., K.S. Novakowski, and P.A. Lapcevic (1988), Interpretation of field tracer tests of a single fracture using a transient solute storage model, *Water Resour. Res., 24*(12), 2019-2032.

Rugh, D.F. and T.J. Burbey (2008), Using saline tracers to evaluate preferential recharge in fractured rocks, Floyd County, Virginia, USA, *Hydrogeol. J., 16*(2), 251-262.

Seaton, W.J. and T.J. Burbey (2000), Aquifer characterization in the Blue Ridge physiographic province using resistivity profiling and borehole geophysics: geologic analysis, *J. Environ. Eng. Geoph., 5*(3), 45-58.

Seaton, W.J. and T.J. Burbey (2002), Evaluation of two-dimensional resistivity methods in a fractured crystalline-rock terrane, *J. Appl. Geophys., 51*, 21-41.

Seaton, W.J. and T.J. Burbey (2005), Influence of ancient thrust faults on the hydrogeology of the Blue Ridge province, *Ground Water, 43*(3), 301-313.

Streltsova, T.D. (1988), *Well testing in heterogeneous formations*. John Wiley and Sons, New York, 413 p.

United States Department of Agriculture (USDA) Soil Survey Staff, Natural Resources Conservation Service (2014), *Web Soil Survey*. http://websoilsurvey.nrcs.usda.gov, accessed June 24, 2014.

U.S. Department of Energy (USDOE) (2014), *Hydraulic Fracturing Technology,* http://energy.gov/fe/hydraulic-fracturing-technology, accessed May 30, 2014.

White, B.A. and T.J. Burbey (2007), Evidence for structurally controlled recharge in the Blue Ridge province, Virginia, USA, *Hydrogeol. J., 15*, 929-943.

Appendix A. Electrical conductivity to Br^- concentration conversion data.

Table 1. Conductivity vs. bromide concentration in each background sample.

Sample 1105-4		Sample 1106-4	
Br^- Concentration (kg/m^3)	Conductivity (µS/cm)	Br^- Concentration (kg/m^3)	Conductivity (µS/cm)
0	103	0	113
0.71	1105	0.51	850
1.72	2540	0.99	1550
2.95	4240	1.63	2455
3.24	4630	2.14	3170
4.42	6205	2.58	3775
5.82	8040	3.08	4425
		4.02	5700
		5.24	7310
		5.94	8236

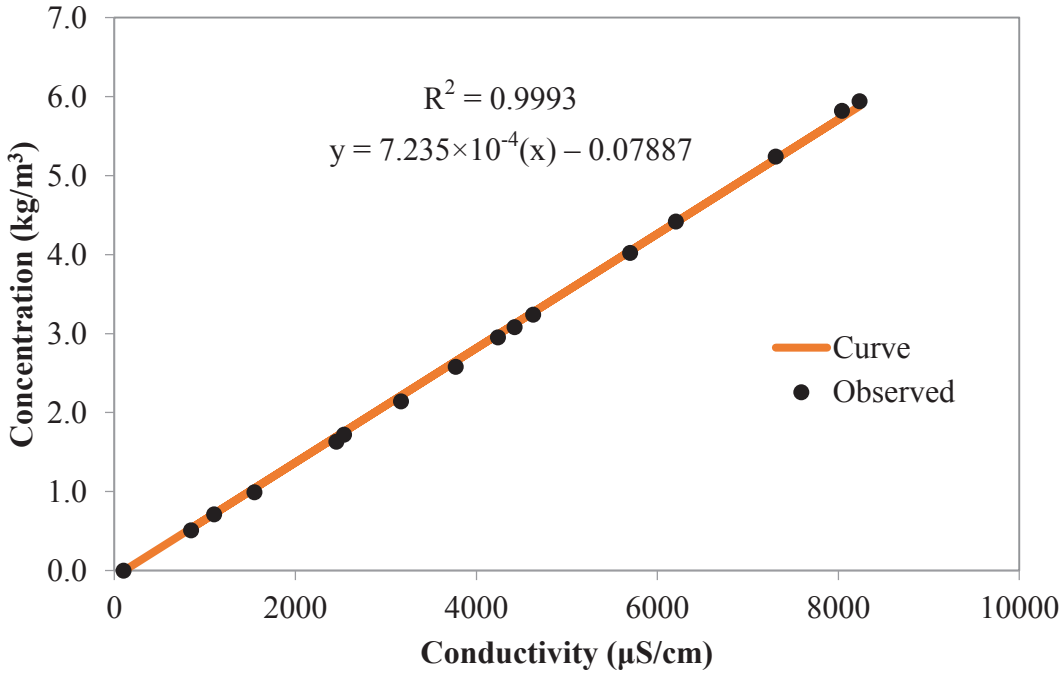

Figure 1. Conductivity-to-concentration curve and experimental data points for Br^-. The x-intercept was forced to be the measured background conductivity on the day of the tracer test (i.e., 109 µS/cm).